Computer-Aided Infarction Identification from Cardiac CT Images: A Biomechanical Approach with SVM*

Ken C.L. Wong[1], Michael Tee[1,3], Marcus Chen[2], David A. Bluemke[1], Ronald M. Summers[1], and Jianhua Yao[1]

[1] Radiology and Imaging Sciences, Clinical Center, NIH, Bethesda, MD, USA
[2] Cardiovascular and Pulmonary Branch, NHLBI, NIH, Bethesda, MD, USA
[3] Institute of Biomedical Engineering, University of Oxford, Oxford, UK

Abstract. Compared with global measurements such as ejection fraction, regional myocardial deformation can better aid detection of cardiac dysfunction. Although tagged and strain-encoded MR images can provide such regional information, they are uncommon in clinical routine. In contrast, cardiac CT images are more common with lower cost, but only provide motion of cardiac boundaries and additional constraints are required to obtain the myocardial strains. To verify the potential of contrast-enhanced CT images on computer-aided infarction identification, we propose a biomechanical approach combined with the support vector machine (SVM). A biomechanical model is used with deformable image registration to estimate 3D myocardial strains from CT images, and the regional strains and CT image intensities are input to the SVM classifier for regional infarction identification. Cross-validations on ten canine image sequences with artificially induced infarctions showed that the normalized radial and first principal strains were the most discriminative features, with respective classification accuracies of $87\pm13\%$ and $84\pm10\%$ when used with the normalized CT image intensity.

1 Introduction

Compared with global cardiac measurements such as wall thickening or ejection fraction, regional myocardial deformation has the potential for early quantification and identification of cardiac dysfunction, especially for myocardial infarction [4]. Cardiac magnetic resonance (MR) imaging techniques such as tagged and strain-encoded imaging are useful in this aspect as they can reveal local myocardial deformation [13], but they are uncommon in clinical routine and relatively expensive. Furthermore, the long breath-hold acquisition time also limits the image quality. In contrast, cardiac computed tomographic (CT) images are more commonly available with lower cost, and a high-resolution image sequence can be produced in just a single heartbeat [8]. However, CT imaging associates with potential radiation risks. Moreover, as CT images can only provide motion of salient features such as the cardiac boundaries, additional constraints are required to estimate the myocardial deformation [13].

Despite the extensive studies of cardiac images in disease diagnosis [4], [9], [6], there are only limited frameworks proposed for computer-aided infarction identification, and most of them are for MR images. In [12], regional 2D myocardial strains and rotation

N. Navab et al. (Eds.): MICCAI 2015, Part II, LNCS 9350, pp. 144–151, 2015.
DOI: 10.1007/978-3-319-24571-3_18

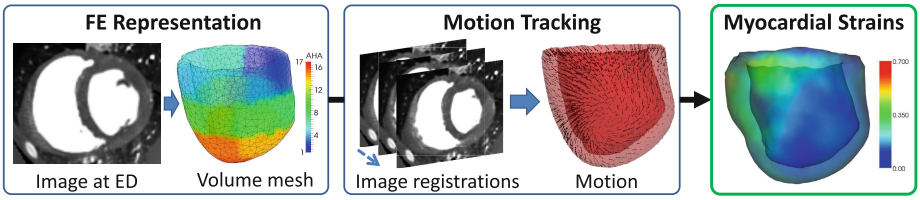

Fig. 1. Biomechanics-based myocardial strain estimation.

angles were estimated from each 2D tagged MR image sequence using nontracking-based estimation. By combining these spatiotemporal measurements into a matrix, a tensor-based linear discriminant analysis framework was proposed to verify whether a heart is normal or diseased. In [11], spatiotemporal measurements of the endocardium and epicardium were extracted from each 2D cine MR image sequence at different ventricular levels using image registration. By using the Shannon's differential entropies of these patterns, a naive Bayes classifier was used to identify regional infarction. To the best of our knowledge, there are currently no computer-aided infarction identification frameworks specifically proposed for CT images.

To study the potential of the clinically more common contrast-enhanced CT images on computer-aided regional infarction identification, we propose a biomechanical approach combined with the support vector machine (SVM) as the classifier. To estimate 3D myocardial strains, displacements of the cardiac boundaries are computed using deformable image registration. By applying these boundary displacements to a finite element (FE) heart representation with hyperelastic and isotropic material properties, the strains are computed by solving the cardiac system dynamics. Apart from strains, CT image intensity which has been shown to be correlated to infarction is also utilized [9]. For regional identification, the left ventricle is divided into 17 zones of the American Heart Association (AHA) nomenclature [1], and the zonal strains and image intensities are input to the SVM classifier. To assess the identification capability, leave-one-subject-out (LOSO) cross-validations were performed on ten canine cardiac image sequences with artificially induced infarctions, and the performances of using different feature combinations were studied.

2 Myocardial Strain Estimation from CT Images

Myocardial strain estimation can be achieved through biomechanics and deformable image registration (Fig. 1). To obtain the FE heart representation, manual segmentation is performed on the end-diastolic image to provide the tetrahedral mesh of the left ventricle which is partitioned into the 17 zones of the AHA nomenclature [1]. With the displacement boundary conditions from image registration, the FE mesh is deformed through the biomechanical model to estimate the myocardial strains.

2.1 Displacement Boundary Conditions by Deformable Image Registration

Image-derived displacement boundary conditions are required to deform the FE mesh. Because of the high image quality of single-heartbeat contrast-enhanced CT images,

motion tracking algorithms developed for cine MR images can be adopted [13]. During the initial framework development, the block-matching method which compares local image blocks between consecutive images was used. Without additional constraints, the resulting displacement fields are unsmooth and physically unrealistic deformation may occur, and thus filtering techniques or manual adjustments are required. In consequence, to facilitate clinical applications, B-spline deformable image registration is used instead [10]. This approach provides smooth deformation fields because of the nature of the B-spline interpolation, and its ITK implementation can provide robust inputs to our biomechanics-based strain estimation.

2.2 Biomechanics-Based Myocardial Strain Estimation

As the displacement fields from image registration can only provide useful information of the salient features such as the cardiac boundaries, to estimate the myocardial strains, deformable models are required. Among different algorithms [13], biomechanics-based approaches have shown promising performance because of the physically realistic constraints such as smooth deformation and tissue incompressibility. Although the heart tissue is known to be orthotropic [3], we use the isotropic material property because subject-specific tissue structures are clinically unavailable. Furthermore, the hyperelastic material property is used as it is more realistic for soft tissues which undergo large deformation [3]. For simplicity, we use the modified Saint-Venant-Kirchhoff constitutive law to model the tissue as nearly incompressible and isotropic material [7]:

$$\psi(\boldsymbol{\epsilon}) = \frac{1}{2}\lambda(J-1)^2 + \mu \mathrm{Tr}(\bar{\boldsymbol{\epsilon}}^2) \tag{1}$$

where $J = \det \mathbf{F}$, with $\mathbf{F}$ the deformation gradient tensor. $\bar{\boldsymbol{\epsilon}}$ is the isovolumetric part of the Green-Lagrange strain tensor $\boldsymbol{\epsilon} = \frac{1}{2}(\mathbf{F}^{\mathrm{T}}\mathbf{F} - \mathbf{I})$. λ and μ are the bulk and shear modulus, respectively. With (1), the second Piola-Kirchhoff stress tensor ($\frac{\partial \psi}{\partial \boldsymbol{\epsilon}}$) and the elasticity tensor ($\frac{\partial^2 \psi}{\partial \boldsymbol{\epsilon}^2}$) can be computed, which are embedded to the FE-based total-Lagrangian cardiac system dynamics for the myocardial deformation [14]:

$$\mathbf{M}\ddot{\mathbf{U}} + \mathbf{C}\dot{\mathbf{U}} + \mathbf{K}\Delta\mathbf{U} = \mathbf{F}_b - \mathbf{F}_t \tag{2}$$

with $\mathbf{M}$, $\mathbf{C}$, and $\mathbf{K}$ the mass, damping, and stiffness matrix, respectively. $\Delta\mathbf{U}$, $\dot{\mathbf{U}}$, and $\ddot{\mathbf{U}}$ contain the nodal incremental displacements, velocities, and accelerations, respectively. $\mathbf{F}_b$ contains the displacement boundary conditions from image registration, and $\mathbf{F}_t$ contains the internal stresses. By solving (2), the nodal displacements and thus strains can be estimated from the image-derived motion. At each node, the three principal strains ($\epsilon_1 > \epsilon_2 > \epsilon_3$) and the six cylindrical strains with respect to the long-axis of the left ventricle (ϵ_{rr}, $\epsilon_{\theta\theta}$, ϵ_{zz}, $\epsilon_{r\theta}$, ϵ_{rz}, $\epsilon_{\theta z}$, with r, θ, and z the radial, circumferential, and longitudinal direction, respectively) are computed for the whole cardiac cycle.

3 Infarction Identification Using SVM

SVM is used to identify infarction from the image-derived features [2]. SVM is a supervised learning algorithm frequently used in medical image analysis because of its

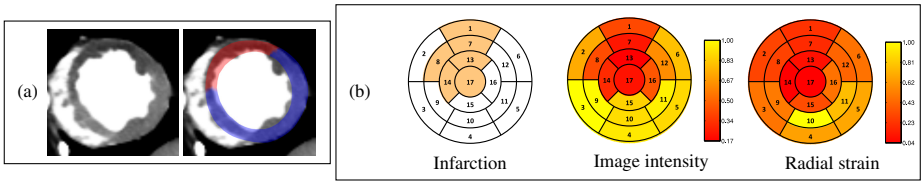

Fig. 2. Data example. (a) Short-axis slice and expert-identified infarction in red (zone 7 and 8). (b) Expert-identified infarction, normalized image intensity, and normalized radial strain (ϵ_{rr}) in terms of AHA zones.

accuracy and flexibility in adapting different sources of data. In a binary classification problem, given training feature vectors with known labels, the SVM classifier constructs a hyperplane whose distances to the nearest training vectors of each class are maximized. Experimentally verified features are used, which include myocardial strains and contrast-enhanced CT image intensity.

3.1 Contrast-Enhanced CT Image Intensity

The capability of using contrast-enhanced CT image intensity to depict myocardial infarction has been verified through experiments [9]. To obtain contrast-enhanced CT images, an iodine-based contrast agent which causes greater absorption and scattering of X-ray radiation is injected into the subject, which leads to an increase in CT attenuation and thus contrast enhancement. As infarction reduces myocardial blood supply, hypo-enhancement can be observed (e.g. Fig. 2(a)). The correlation between the hypo-enhanced and infarcted regions was validated through porcine data with postmortem TTC staining [9]. As hypo-enhancement lasts for several cardiac cycles, it can be a robust feature for infarction identification. In our framework, as regional infarction is of interest, the average value of the image intensities at the bottom 10th percentile of each AHA zone at end-diastole is used (Fig. 2(b)). To alleviate the effects of inter-subject variability and to facilitate the accuracy and stability of the SVM classifier, the AHA zonal intensities are normalized (divided) by the largest zonal intensity of each subject.

3.2 Myocardial Strains

The capability of using strains to identify infarction has been verified from animal and human data, with the strain magnitude inversely proportional to the infarction severity [4], [6]. Strains estimated from tagged MR images show their superiority to wall thickening [4], and strains estimated by speckle tracking echocardiography correlate well with the normal and abnormal cardiac functions including infarction [6]. In our framework, the AHA zonal strains estimated by the biomechanical model are used, which are computed as the average nodal strains of the zones. For each strain type (e.g. ϵ_{rr}) in each zone, the zonal strain with the largest magnitude in the whole cardiac cycle is used as a SVM instance. To alleviate the effects of inter-subject variability, for each strain type, the zonal strains are normalized (divided) by the largest zonal strain magnitude among all zones in the whole cardiac cycle of each subject (Fig. 2(b)). The differences between using normalized and unnormalized strains are presented in Section 4.

Table 1. F-scores of normalized and unnormalized features.

	ϵ_{rr}	$\epsilon_{\theta\theta}$	ϵ_{zz}	$\epsilon_{r\theta}$	ϵ_{rz}	$\epsilon_{\theta z}$	ϵ_1	ϵ_2	ϵ_3	Intensity
Normalized	0.79	0.42	0.06	0.00	0.11	0.00	0.59	0.07	0.17	0.48
Unnormalized	0.36	0.37	0.05	0.00	0.13	0.00	0.21	0.05	0.07	0.29

3.3 SVM and Cross-Validations

The SVM C-support vector classification which is less sensitive to outliers is utilized [2]. We use the linear kernel because it gave similar results as the nonlinear kernels in our experiments but was more computationally efficient. Grid search is used to select the optimal regularization parameter C using the training data.

To verify the capabilities of different feature combinations on infarction identification, LOSO cross-validations are used. Let n be the number of subjects. In each test, the zonal features of $n-1$ subjects are used to train the classifier, which is then used to classify the zonal infarction of the left-out subject. The average performance can then be obtained after the n tests. The classification accuracy ($\in$ [0,1]) of each LOSO test is defined as (# of correctly identified zones) / (# of zones). For the inter-rater agreement between the ground truth and the classification, the Gwet's AC1 coefficient ($\in$ [-1,1]), which has been shown to be more reliable than the Cohen's kappa, is used [5].

Moreover, to measure feature discrimination, a variant of Fisher score is used [2]:

$$\text{F-score} = \frac{\left(\bar{x}^{(+)} - \bar{x}\right)^2 + \left(\bar{x}^{(-)} - \bar{x}\right)^2}{\frac{1}{n_+ - 1}\sum_{i=1}^{n_+}\left(x_i^{(+)} - \bar{x}^{(+)}\right)^2 + \frac{1}{n_- - 1}\sum_{i=1}^{n_-}\left(x_i^{(-)} - \bar{x}^{(-)}\right)^2} \tag{3}$$

with $\bar{x}$, $\bar{x}^{(+)}$, and $\bar{x}^{(-)}$ the average value of the whole, positive-labeled (infarct), and negative-labeled (normal) instances of a feature, respectively. n_+ and n_- are the numbers of positive and negative instances, and $x_i^{(+)}$ and $x_i^{(-)}$ are the ith positive and negative instances. Therefore, a larger F-score means a more discriminative feature.

4 Experiments

4.1 Experimental Setups

Ten single-heartbeat contrast-enhanced CT image sequences of ten canines with artificially induced myocardial infarctions were acquired by the Toshiba Aquilion ONE CT system, with the infarctions caused by left anterior descending artery blockages. Each cardiac cycle (0.52-0.96s) had 20 frames, with voxel size of $0.28 \times 0.28 \times 1.00$ mm^3. The infarcted regions were identified by experts using dynamic perfusion CT images in terms of AHA zones, with 110 normal and 60 infarcted zones in total. Different feature combinations were studied, including using the strains separately (single-strain) or altogether (all-strain), and with or without using normalization and image intensity. As the control group without infarction was unavailable, the capability of the framework on discriminating between infarcted and non-infarcted hearts could not be studied.

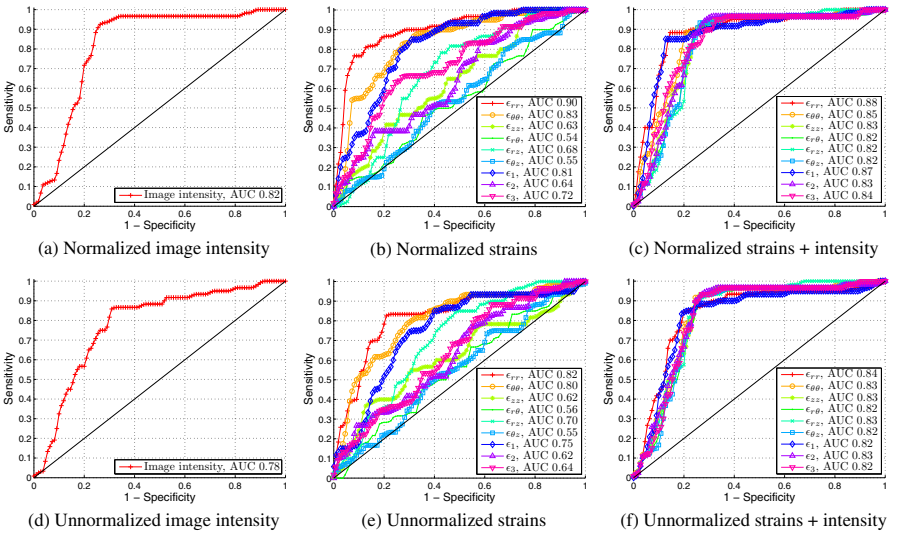

(a) Normalized image intensity (b) Normalized strains (c) Normalized strains + intensity

(d) Unnormalized image intensity (e) Unnormalized strains (f) Unnormalized strains + intensity

Fig. 3. Single-strain features. Average ROC curves of LOSO cross-validations. Each curve was constructed from the SVM decision values of all tests in a cross-validation. In (c) and (f), only the normalized image intensity was used with the strains.

Table 2. Single-strain features. Results of LOSO cross-validations. For normalized image intensity, accuracy = 81±16% and AC1 = 63±32%. For unnormalized image intensity, accuracy = 74±24% and AC1 = 52±44%. Only the normalized image intensity was used with the strains.

		ϵ_{rr}	$\epsilon_{\theta\theta}$	ϵ_{zz}	$\epsilon_{r\theta}$	ϵ_{rz}	$\epsilon_{\theta z}$	ϵ_1	ϵ_2	ϵ_3
Normalized strains										
Strains	Accuracy (%)	84±11	79±9	66±14	58±15	66±8	56±16	72±15	58±15	71±10
	AC1 (%)	71±20	65±14	40±28	34±30	37±17	30±37	47±30	34±30	45±21
Strains + intensity	Accuracy (%)	87±13	80±14	80±16	80±16	79±17	80±16	84±10	79±18	77±15
	AC1 (%)	75±25	61±28	62±32	62±31	61±32	62±32	69±20	60±33	56±30
Unnormalized strains										
Strains	Accuracy (%)	76±17	75±10	64±11	58±15	65±10	57±15	68±20	58±15	59±14
	AC1 (%)	54±34	57±21	36±22	34±30	33±21	31±35	40±36	34±30	36±29
Strains + intensity	Accuracy (%)	80±20	81±17	80±16	80±16	80±16	79±16	80±20	80±16	79±16
	AC1 (%)	62±38	64±32	62±32	62±31	62±32	61±31	62±37	62±31	61±31

4.2 Results

Table 1 shows the F-scores of the normalized and unnormalized features. The radial (ϵ_{rr}), circumferential ($\epsilon_{\theta\theta}$), and first principal (ϵ_1) strains were more discriminative than the other strains, regardless of normalization. This finding is consistent with the literature [4], [6]. With normalization, the F-scores were improved in general and those of ϵ_{rr} and ϵ_1 were more than doubled. The small F-scores of the shear and longitudinal strains are consistent with the fact that twisting and long-axis motions cannot be properly revealed by CT images. The F-score of the normalized image intensity (0.48)

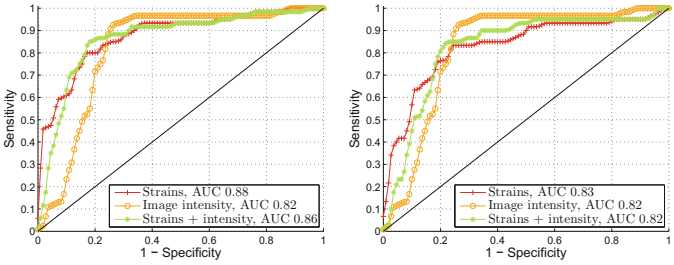

(a) Normalized strains (b) Unnormalized strains

Fig. 4. All-strain features. Average ROC curves of LOSO cross-validations. Each curve was constructed from the SVM decision values of all tests in a cross-validation. Only the normalized image intensity was used.

Table 3. All-strain features. Results of LOSO cross-validations. For the normalized image intensity, accuracy = 81±16% and AC1 = 63±32%. Only the normalized image intensity was used.

		Normalized strains	**Unnormalized strains**
Strains	Accuracy (%)	79±10	74±18
	AC1 (%)	61±19	50±34
Strains + intensity	Accuracy (%)	83±12	80±17
	AC1 (%)	67±24	63±32

was larger than the unnormalized one (0.29), and it was also larger than those of the unnormalized strains but comparable to those of the more discriminative normalized strains. These show that the proposed feature normalization in Section 3 for alleviating inter-subject variability can improve the identification performance.

Fig. 3 and Table 2 show the results of using the single-strain features. The classification capabilities were consistent with the F-scores. The capability of the normalized image intensity was better than those of the unnormalized strains as indicated by the area under curve (AUC) (Fig. 3(a) and (e)) and other measures (Table 2). When using the normalized image intensity with the unnormalized strains (Fig. 3(f)), the normalized image intensity was dominant and thus the unnormalized strains were unnecessary. On the other hand, the normalized ϵ_{rr} (Fig. 3(b)) outperformed the normalized image intensity. When combining with the normalized image intensity (Fig. 3(c)), both the normalized ϵ_{rr} and the normalized ϵ_1 outperformed themselves and the normalized image intensity alone, and the performance of the normalized ϵ_1 became similar to that of the normalized ϵ_{rr}. This is an important observation as ϵ_1 is simpler to compute and is more robust without the need to define the long-axis of the left ventricle.

Fig. 4 and Table 3 show the results of using the all-strain features. Similar to the single-strain features, the normalized strains outperformed the unnormalized ones. The combination of the normalized image intensity and the unnormalized strains was similar to using the normalized image intensity alone. The combination of the normalized image intensity and the normalized strains gave the best results, however, its performance (Table 3) was worse than those using the normalized ϵ_{rr} or the normalized ϵ_1 with image intensity (Table 2). These show that the use of all strains is unnecessary.

5 Conclusion

We have presented a biomechanics-based computer-aided framework to identify myocardial infarction from cardiac CT images. Regional CT image intensities and myocardial strains, whose correlations with infarction have been experimentally verified, are used with SVM to achieve promising identification performance. Experimental results showed that the normalized features outperformed the unnormalized ones, and the normalized radial strain and the normalized first principal strain were the most discriminative strain features when combined with the normalized image intensity.

References

1. Cerqueira, M.D., Weissman, N.J., Dilsizian, V., Jacobs, A.K., Kaul, S., Laskey, W.K., Pennell, D.J., Rumberger, J.A., Ryan, T., Verani, M.S.: Standardized myocardial segmentation and nomenclature for tomographic imaging of the heart: a statement for healthcare professionals from the cardiac imaging committee of the Council on Clinical Cardiology of the American Heart Association. Circulation 105(4), 539–542 (2002)
2. Chen, Y.W., Lin, C.J.: Combining SVMs with various feature selection strategies. In: Guyon, I., Nikravesh, M., Gunn, S., Zadeh, L.A. (eds.) Combining SVMs with Various Feature Selection Strategies. STUDFUZZ, vol. 207, pp. 315–324. Springer, Heidelberg (2006)
3. Glass, L., Hunter, P., McCulloch, A. (eds.): Theory of Heart: Biomechanics, Biophysics, and Nonlinear Dynamics of Cardiac Function. Springer (1991)
4. Götte, M.J.W., van Rossum, A.C., Twisk, J.W.R., Kuijer, J.P.A., Tim Marcus, J., Visser, C.A.: Quantification of regional contractile function after infarction: strain analysis superior to wall thickening analysis in discriminating infarct from remote myocardium. Journal of the American College of Cardiology 37(3), 808–817 (2001)
5. Gwet, K.L.: Computing inter-rater reliability and its variance in the presence of high agreement. British Journal of Mathematical and Statistical Psychology 61(1), 29–48 (2008)
6. Hoit, B.D.: Strain and strain rate echocardiography and coronary artery disease. Circulation: Cardiovascular Imaging 4(2), 179–190 (2011)
7. Holzapfel, G.A.: Nonlinear Solid Mechanics: A Continuum Approach for Engineering. John Wiley & Sons, Inc. (2000)
8. Hsiao, E.M., Rybicki, F.J., Steigner, M.: CT coronary angiography: 256-slice and 320-detector row scanners. Current Cardiology Reports 12(1), 68–75 (2010)
9. Mahnken, A.H., Bruners, P., Katoh, M., Wildberger, J.E., Günther, R.W., Buecker, A.: Dynamic multi-section CT imaging in acute myocardial infarction: preliminary animal experience. European Radiology 16(3), 746–752 (2006)
10. Pluim, J.P.W., Maintz, J.B.A., Viergever, M.A.: Mutual-information-based registration of medical images: a survey. IEEE Transactions on Medical Imaging 22(8), 986–1004 (2003)
11. Punithakumar, K., Ayed, I.B., Islam, A., Goela, A., Ross, I.G., Chong, J., Li, S.: Regional heart motion abnormality detection: an information theoretic approach. Medical Image Analysis 17(3), 311–324 (2013)
12. Qian, Z., Liu, Q., Metaxas, D.N., Axel, L.: Identifying regional cardiac abnormalities from myocardial strains using nontracking-based strain estimation and spatio-temporal tensor analysis. IEEE Transactions on Medical Imaging 30(12), 2017–2029 (2011)
13. Wang, H., Amini, A.A.: Cardiac motion and deformation recovery from MRI: a review. IEEE Transactions on Medical Imaging 31(2), 487–503 (2012)
14. Wong, K.C.L., Wang, L., Zhang, H., Liu, H., Shi, P.: Physiological fusion of functional and structural images for cardiac deformation recovery. IEEE Transactions on Medical Imaging 30(4), 990–1000 (2011)